Advances in Aircraft and Spacecraft Science, *Vol. 9, No. 3 (2022) 217-242*
https://doi.org/10.12989/aas.2022.9.3.217

A micromechanics-based time-domain viscoelastic constitutive model for particulate composites: Theory and experimental validation

Hangil You[1], Hyoung Jun Lim[1] and Gun Jin Yun*[1,2]

[1]*Department of Aerospace Engineering, Seoul National University, Gwanak-gu, Seoul, 08826, South Korea*
[2]*Institute of Advanced Aerospace Technology, Seoul National University, 08826, Seoul, South Korea*

(Received February 9, 2022, Revised May 11, 2022, Accepted May 18, 2022)

Abstract. This paper proposes a novel time-domain homogenization model combining the viscoelastic constitutive law with Eshelby's inclusion theory-based micromechanics model to predict the mechanical behavior of the particle reinforced composite material. The proposed model is intuitive and straightforward capable of predicting composites' viscoelastic behavior in the time domain. The isotropization technique for non-uniform stress-strain fields and incremental Mori-Tanaka schemes for high volume fraction are adopted in this study. Effects of the imperfectly bonded interphase layer on the viscoelastic behavior on the dynamic mechanical behavior are also investigated. The proposed model is verified by the direct numerical simulation and DMA (dynamic mechanical analysis) experimental results. The proposed model is useful for multiscale analysis of viscoelastic composite materials, and it can also be extended to predict the nonlinear viscoelastic response of composite materials.

Keywords: Eshelby inclusion theory; homogenization; micromechanics; particulate composite; viscoelastic material

1. Introduction

Demands of lightweight and durable composite materials have ever increased in aerospace industries for their high specific stiffness, strength, damping characteristics, etc. Complex behavior of polymer matrix composites under high-temperature and cyclic thermomechanical loadings has posed challenges on the predictive modeling of viscoelastic behavior, despite various advantages that the mechanical properties are adjustable according to the composite composition and applications of functional nanomaterials. The experimental evaluation of the effective properties of the composites is expensive and time-consuming. Therefore, computational prediction models for effective properties of the composites have been required and researched. A variety of computational micromechanics models for carbon nanotube (CNT)/polymer (Li *et al.* 2006, Shokrieh *et al.* 2016, Kolahchi and Cheraghbak 2017, Patnaik *et al.* 2020), carbon black/rubber (Liu 2017, Jung *et al.* 2021), carbon black/shape memory polymer (SMP) (Pan *et al.* 2019, Zhao *et al.* 2019), porous polymer (Le *et al.* 2007), and fiber reinforced concrete (Dutra *et al.* 2010), have been suggested with

*Corresponding author, Professor, E-mail: gunjin.yun@snu.ac.kr

http://www.techno-press.org/?journal=aas&subpage=7 ISSN: 2287-528X (Print), 2287-5271 (Online)

a wide range of predictive capabilities and modeling efficiencies.

Among the composites' material systems, composites consisting of viscoelastic matrix and stiff particles have been widely used in engineering applications due to their excellent combination of high stiffness, damping, and light-weight properties (Paipetis and Grootenhuis 1979, Zhu *et al.* 2014, Hu *et al.* 2018). Micromechanical constitutive models for predicting the particulate composites' effective viscoelastic properties are still under active research and development. According to the literature, the viscoelastic constitutive models for the particulate composites can generally be classified into two categories: 1) the homogenization in the Laplace domain and 2) homogenization in the time domain.

The initial contribution to the homogenization modeling framework based on the Laplace Transformation was pioneered by Hashin (1965) in 1965. Hashin proposed a set of homogenization procedures in the Laplace domain whereby the equations are transformed inversely to the time-domain to obtain the composites' effective responses. According to the correspondence principle, the Laplace Transformation enabled the linearization of the nonlinear mechanical response of viscoelastic materials over time. Therefore, the simple homogenization schemes could be applied to linearized mechanical properties in the Laplace domain. Followed by Hashin's work, various micromechanical schemes in the Laplace domain were proposed, such as the self-consistent method (Laws and McLaughlin 1978), the Mori-Tanaka method (Brinson and Lin 1998), or the Hashin-Shtrikman bounds (DeBotton and Tevet-Deree 2004). Various homogenization methods were used in the Laplace domain to evaluate the complex modulus (Christensen 1969, Hashin 1970, Li and Weng 1994) and damping properties (Dunn 1995) of linear viscoelastic particulate composites. Brinson *et al*. also proposed a micromechanical model to predict a three-phase viscoelastic composite's mechanical property with Mori-Tanaka theory (Fisher and Brinson 2001). Azoti *et al*. presented a micromechanical model to analyze the viscoelastic composites' damping response by transforming the viscoelastic equation to the Carson-Laplace transform domain (Azoti *et al.* 2013). Previous studies on homogenization based on Laplace transformation have provided a great advantage in analyzing the viscoelastic composites' effective frequency-dependent properties. However, homogenization based on Laplace transformation has some limitations. The main limitation is that the Laplace domain's homogenization solution is usually difficult to invert back to the time domain. This is because the Laplace domain's homogenization solution is not always in a closed form or is not simple enough to be analytically inverted (Chen *et al.* 2020). Therefore, effective mechanical properties in the time domain can be obtained with simplification of models (Hashin 1965) or through numerical inversion of the Laplace transformation (Brenner *et al.* 2002), a computationally expensive operation. An approximate inversion method has been proposed to increase accuracy (Brenner *et al.* 2002) but is limited to monotonic loading for good accuracy.

To overcome the limitations above, a few homogenization methods in the time domain have been proposed to characterize the interaction between inclusions and homogeneous media for viscoelastic particulate composites (Escarpini Filho and Marques 2016, Rodríguez-Ramos *et al.* 2020). Molinari *et al*. proposed self-consistent schemes considering the interaction with additive-interaction law to evaluate composites' time-dependent viscoplastic behavior (Molinari *et al.* 1997). Berbenni *et al*. presented a time-incremental internal variable homogenization scheme for viscoelastic composites considering the interaction with an exact-interaction solution (Berbenni *et al.* 2015). Their approach could consider the interaction between inclusions and matrix in the time domain. However, the closed-form constitutive equation for the composites could not be obtained. For other time-domain homogenization approaches such as variation of incremental methods, Lahellec proposed an approximate scheme for estimating the effective response of linear viscoelastic composites directly

in the time-domain (Lahellec and Suquet 2007). An incremental internal variables approach was first proposed in this research. Ricaud *et al*. presented an incremental formulation that combines the Laplace transform with internal variables (Ricaud and Masson 2009). Their approach was able to obtain the exact effective behavior for two-phase microstructure based on the collocation method and an internal variable formulation. Recently, Chen *et al*. presented a micromechanics-based homogenization model with explicitly closed-form constitutive equations (Chen *et al.* 2020). Their work provided the closed-form constitutive equation for the viscoelastic particulate composite in the time domain. Sevostianov *et al*. presented a homogenization method to predict effective viscoelastic properties of a short fiber reinforced composite. They utilized fraction-exponential operators of Scoot Blair-Rabotnov for the convenience of inverse Laplace transformation (Sevostianov *et al.* 2016). Unlike models based on the Laplace transform, the time domain homogenization method can provide an explicit effective mechanical response of viscoelastic composites. However, it is very difficult to obtain the closed constitutive equation of viscoelastic composites in those time domain homogenization methods due to the time-dependent material characteristics. Recently, Kim *et al*. proposed a novel adaptive affine homogenization method for visco-hyperelastic composites that effective stress can be predicted on the time domain. In this research, the adaptive affine method is proposed to resolve inconsistency between the strain concentration tensor and accumulated strain (Kim *et al.* 2022). Compared with the present study, they used the adaptive affine method to correct for each time step strain because the strain is huge as a viscoelastic model.

In this paper, a novel time-domain homogenization method is proposed to obtain the explicit mechanical response of linear viscoelastic particulate composites over time by combining the Mori-Tanka method viscoelastic constitutive equation. We utilized the Mori-Tanaka theory to homogenize the composite's compliance matrix at each time increment and calculate the stress by numerically integrating the effective compliance matrix and strain over time. Unlike the homogenization methods in the time domain discussed above, the effective compliance matrix that considers the inclusion shape and interaction is obtained, and stresses at a specific time are evaluated with the obtained compliance matrix and strain rate only. This intuitive and straightforward approach can obtain the homogenized stress in the time domain by numerical integrations of the Boltzman integral equation with a homogenized constitutive matrix over time. This approach was not previously reported and has unique contributions on obtaining time-domain solutions for viscoelastic composite with Mori-Tanaka approaches. For instance, time-domain solution for any input loading with varying frequencies can be obtained with the proposed methodology.

In Section 2, the micro-mechanical model's fundamental is introduced, and the constitutive model of Mori-Tanaka viscoelastic material is presented. The numerical implementation of the proposed homogenization model is also introduced with a comprehensive flowchart and pseudocodes. In Section 3, direct numerical simulation (DNS) using the commercial software ABAQUS is performed to verify the proposed time-domain homogenization model. The proposed homogenization model considering the interphase layer is also investigated for further verification. In Section 4, the experiments for stress relaxation and dynamic mechanical properties are conducted to compare the proposed homogenization results with experiments. Finally, conclusions were summarized in Section 5, along with future research directions.

2. Constitutive modeling of the micromechanical model

This section presents the constitutive modeling procedure for the proposed homogenization

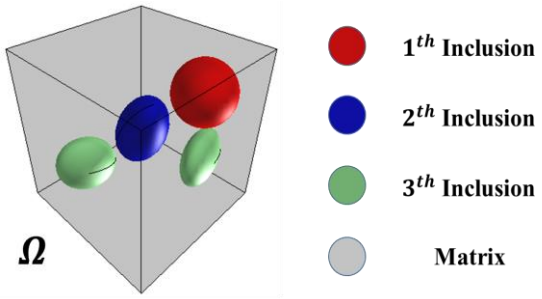

Fig. 1 RVE of the particulate composite

model with continuum mechanics theory. The homogenization by Eshelby's inclusion theory is introduced and the constitutive model of Mori-Tanaka viscoelastic material is shown. Lastly, the numerical implementation of the proposed homogenization model is introduced.

2.1 Homogenization approach by Eshelby's inclusion theory

Consider the particulate composite material that consists of materials of N+1 phases. To estimate this composite material's effective properties, a Representative Volume Element (RVE) of the particulate composite is considered as shown in Fig. 1. Here, $\boldsymbol{\varepsilon}_{micro}(\vec{\boldsymbol{r}})$ is the microscopic strain tensor at an arbitrary location $(\vec{\boldsymbol{r}})$ within the RVE and $\boldsymbol{\varepsilon}_{macro}$ is the far-field macroscopic strain tensor that acts on the boundaries of the RVE. The global strain concentration tensor $\boldsymbol{B}(\vec{\boldsymbol{r}})$ at an arbitrary location $\vec{\boldsymbol{r}}$ contains the information of the microstructure and links the microscopic strain to the macroscopic strain as follows (Vieville *et al.* 2006)

$$\varepsilon_{micro}(\vec{r}) = B(\vec{r}) : \varepsilon_{macro} \tag{1}$$

Typically, the global strain concentration tensor $\boldsymbol{B}(\vec{\boldsymbol{r}})$ is obtained iteratively. To explain the procedure, we introduce the local strain concentration tensor $\boldsymbol{b}(\vec{\boldsymbol{r}})$ in Eq. (2).

$$\varepsilon_{micro}(\vec{r}) = b(\vec{r}) : \varepsilon^{r}_{macro} \tag{2}$$

where $\boldsymbol{\varepsilon}^{r}_{macro}$ is the macroscopic strain of the reference medium. Substituting Eq. (2) to $\boldsymbol{\varepsilon}_{macro} = (\frac{1}{\Omega}) \int_{\Omega} \boldsymbol{\varepsilon}_{micro}(\vec{\boldsymbol{r}}) d\Omega$, the relationship between $\boldsymbol{\varepsilon}^{r}_{macro}$ and $\boldsymbol{\varepsilon}_{macro}$ can be derived as follows.

$$\boldsymbol{\varepsilon}^{r}_{macro} = < \boldsymbol{b}(\vec{\boldsymbol{r}}) >^{-1} : \boldsymbol{\varepsilon}_{macro}(\vec{\boldsymbol{r}}) \tag{3}$$

Where the bracket <·> is the volume-averaged quantity. Then, substituting Eq. (3) to Eq. (2), the global strain concentration tensor is obtained as follows

$$\begin{aligned} \boldsymbol{\varepsilon}_{micro}(\vec{\boldsymbol{r}}) &= \boldsymbol{b}(\vec{\boldsymbol{r}}) : < \boldsymbol{b}(\vec{\boldsymbol{r}}) >^{-1} \\ \boldsymbol{\varepsilon}_{macro}(\vec{\boldsymbol{r}}) &= \boldsymbol{B}(\vec{\boldsymbol{r}}) : \boldsymbol{\varepsilon}_{macro}(\vec{\boldsymbol{r}}) \end{aligned} \tag{4}$$

$$\boldsymbol{B}(\vec{\boldsymbol{r}}) = \boldsymbol{b}(\vec{\boldsymbol{r}}) : < \boldsymbol{b}(\vec{\boldsymbol{r}}) >^{-1} \tag{5}$$

Assuming far-field macroscopic strain loads applied to the boundary of the RVE, effective stiffness of the micromechanical model is obtained in terms of the global strain concentration tensor

$\boldsymbol{B}(\vec{\boldsymbol{r}})$ and the local stiffness tensor $\boldsymbol{c}(\vec{\boldsymbol{r}})$ at the arbitrary location $\vec{\boldsymbol{r}}$ by applying the volume averaging method as follows

$$\boldsymbol{C}_{macro}^{eff} = \frac{1}{\Omega}\int_{\Omega} \boldsymbol{c}\,(\vec{\boldsymbol{r}}) : \boldsymbol{B}\,(\vec{\boldsymbol{r}}) d\Omega \tag{6}$$

The local stiffness tensor $\boldsymbol{c}(\vec{\boldsymbol{r}})$ is decomposed into a homogenized part and a fluctuation part that varies according to the location, $\vec{\boldsymbol{r}}$.

$$\boldsymbol{c}(\vec{\boldsymbol{r}}) = \boldsymbol{C}_{macro}^{eff} + \delta \boldsymbol{C}_{fluc}\,(\vec{\boldsymbol{r}}) \tag{7}$$

From Eq. (2) and (7), Eq. (7) can be substituted within the equilibrium equation and therefore enables the derivation of the kinematic integral equation of Dederichs and Zeller. The microscopic strain tensor $\boldsymbol{\varepsilon_{micro}}(\vec{\boldsymbol{r}})$ is expressed with a modified Green tensor $\boldsymbol{\xi}$ as follows (Dederichs and Zeller 1973)

$$\boldsymbol{\varepsilon}_{micro}(\vec{\boldsymbol{r}}) = \boldsymbol{\varepsilon}_{macro}^{r} - \int_{\Omega'} \boldsymbol{\xi}(\vec{\boldsymbol{r}} - \vec{\boldsymbol{r}}') : \delta \boldsymbol{C}_{fluc}\,(\vec{\boldsymbol{r}'}) : \boldsymbol{\varepsilon}_{micro}(\vec{\boldsymbol{r}}\,') d\Omega' \tag{8}$$

By utilizing the mean-field volume average on Eq. (8), the average strain on I^{th} phase is obtained as

$$\bar{\boldsymbol{\varepsilon}}^{I} = \boldsymbol{\varepsilon}_{macro}^{r} - \sum_{J=0}^{N} \frac{1}{\Omega_I}\int_{\Omega_I}\int_{\Omega_J} \boldsymbol{\xi}(\vec{\boldsymbol{r}} - \vec{\boldsymbol{r}_J}) d\Omega_J d\Omega_I : \delta \boldsymbol{C}_{fluc}^{J} : \boldsymbol{\varepsilon}_{micro}^{J} \tag{9}$$

$$\bar{\boldsymbol{\varepsilon}}^{I} = \boldsymbol{\varepsilon}_{macro}^{r} - \sum_{J=0}^{N} \boldsymbol{T}^{IJ} : \delta \boldsymbol{C}_{fluc}^{J} : \boldsymbol{\varepsilon}_{micro}^{J} \tag{10}$$

where N is the number of phases. Fahri *et al*. (Fassi-Fehri 1985) proposed the interaction tensor $\boldsymbol{T}^{IJ}$ that contains the interaction information between I^{th} phase and the J^{th} phase of the composite material. $\boldsymbol{T}^{IJ}$ is expressed as

$$\boldsymbol{T}^{IJ} = \frac{1}{\Omega_I}\int_{\Omega_I}\int_{\Omega_J} \boldsymbol{\xi}\left(\vec{\boldsymbol{r}} - \vec{\boldsymbol{r}_J}\right) d\Omega_J d\Omega_I, \tag{11}$$

Now, we utilize the concept of the local strain tensor $\boldsymbol{b}^{I}(\vec{\boldsymbol{r}})$ that links the homogeneous strain $\boldsymbol{\varepsilon}_{macro}$ to the average strain field within the I^{th} inclusion. For the I^{th} inclusions, the following relationship is satisfied.

$$\boldsymbol{\varepsilon}^{I}(\vec{\boldsymbol{r}}) = \boldsymbol{b}^{I}(\vec{\boldsymbol{r}}) : \boldsymbol{\varepsilon}_{macro}^{r} \tag{12}$$

$$\boldsymbol{B}^{I}(\vec{\boldsymbol{r}}) = \boldsymbol{b}^{I}(\vec{\boldsymbol{r}}) : < \boldsymbol{b}^{I}(\vec{\boldsymbol{r}}) >^{-1} \tag{13}$$

Substituting Eq. (2) to Eq. (10) and enforcing the validity of Eq. (10) for all macroscopic strain $\boldsymbol{\varepsilon}_{macro}^{r}$, the local strain tensor at the (i+1)$^{\text{th}}$ iteration $\boldsymbol{b}_{i+1}^{I}(\vec{\boldsymbol{r}})$ is derived as follows

$$\boldsymbol{b}_{i+1}^{I}(\vec{\boldsymbol{r}}) = [\boldsymbol{I}^{tensor} + \boldsymbol{T}^{II} : (\boldsymbol{C}^{I} - \boldsymbol{C}^{r})]^{-1} :$$

$$\left[\boldsymbol{I}^{tensor} - \sum_{\substack{J=0,\\ J\neq I}}^{N} \boldsymbol{T}^{IJ} : (\boldsymbol{C}^{J} - \boldsymbol{C}^{r}) : \boldsymbol{b}_i^I(\vec{\boldsymbol{r}})\right] \tag{14}$$

here $\boldsymbol{b}_i^I(\vec{\boldsymbol{r}})$ is the approximate local strain concentration tensor of the I^{th} phase at the i-th iteration and $\boldsymbol{I}^{tensor}$ is an identity tensor. Depending on the choice of the reference medium, two approaches exist; 1) Mori-Tanaka approach when $\boldsymbol{C}^r$ is assumed to be $\boldsymbol{C}^0$ (i.e., stiffness of the surrounding matrix) and 2) Self-consistent approach when $\boldsymbol{C}^r$ is assumed to be $\boldsymbol{C}_{macro}^{eff}$. In this paper, we adopted the Mori-Tanaka approach. Therefore, Eq. (10) and (14) change to

$$\bar{\boldsymbol{\varepsilon}}^I = \boldsymbol{\varepsilon}_{macro}^0 - \sum_{J=0}^{N} \boldsymbol{T}^{IJ} : \Delta\boldsymbol{C}^J : \boldsymbol{\varepsilon}_{micro}^J \tag{15}$$

$$\boldsymbol{b}_{\boldsymbol{i+1}}^I(\vec{\boldsymbol{r}}) = [\boldsymbol{I}^{tensor} + \boldsymbol{T}^{II} : (\boldsymbol{C}^I - \boldsymbol{C}^0)]^{-1} : \left[\boldsymbol{I}^{tensor} - \sum_{\substack{J=1,\\ J\neq I}}^{N} \boldsymbol{T}^{IJ} : (\boldsymbol{C}^J - \boldsymbol{C}^0) : \boldsymbol{b}_i^I(\vec{\boldsymbol{r}})\right], \quad I = 0,1,2,\dots,N \tag{16}$$

Herein, $\Delta\boldsymbol{C}^J$ is a difference between the stiffness of fiber phase (J) and the matrix. In a condition that considers the interaction between the individual inclusions and surrounding matrix (i.e., one-site approximation), the interaction tensor $\boldsymbol{T}^{II}$ can be expressed as follows

$$\boldsymbol{T}^{II} = \boldsymbol{S} : (\boldsymbol{C}^0)^{-1} \tag{17}$$

where $\boldsymbol{S}$ is the Eshelby's tensor that contains the information of the inclusion's shape and $\boldsymbol{C}^0$ is the stiffness tensor for matrix phase following the Mori-Tanaka scheme. $\boldsymbol{T}^{IJ}$ is neglected in the one-site approximation, which means the interaction between I and J-th inclusions is not included.

Consequently, the effective stiffness tensor $\boldsymbol{C}_{macro}^{eff}$ from Eq. (6) can be represented with a volume fraction of the I^{th} inclusion v_I and stiffness tensor of I^{th} inclusion $\boldsymbol{C}^I$. It is given as

$$\boldsymbol{C}_{macro}^{eff} = \sum_{I=0}^{N} v_I\, \boldsymbol{C}^I : \boldsymbol{B}^I = v_0 \boldsymbol{C}^0 : \boldsymbol{B}^0 + \sum_{I=1}^{N} v_I\, \boldsymbol{C}^I : \boldsymbol{B}^I = \left[v_0 \boldsymbol{C}^0 + \sum_{I=1}^{N} v_I\, \boldsymbol{C}^I : \boldsymbol{b}^I\right] : \boldsymbol{B}^0 \tag{18}$$

In Eq. (18), the following relationship $\boldsymbol{B}^{\boldsymbol{0}} = \boldsymbol{b}^{\boldsymbol{0}} : <\boldsymbol{b}^I>^{-\boldsymbol{1}} = <\boldsymbol{b}^I>^{-\boldsymbol{1}}$ and $\boldsymbol{B}^I = \boldsymbol{b}^I : <\boldsymbol{b}^I>^{-\boldsymbol{1}} = \boldsymbol{b}^I : \boldsymbol{B}^{\boldsymbol{0}}$ are used assuming the Mori-Tanaka scheme.

2.2 Constitutive model of the Mori-Tanaka viscoelastic material

In this paper, the Generalized Maxwell model is adopted for the viscoelastic behavior of the polymer matrix. The Boltzmann superposition integral for a general viscoelastic constitutive model is expressed in terms of the relaxation modulus as follows

$$\boldsymbol{\sigma}_{ij}(t) = \int_{-\infty}^{t} \boldsymbol{C}_{ijkl}^{VE}(t-\tau) : \frac{\partial \boldsymbol{\varepsilon}_{kl}}{\partial \tau} d\tau \tag{19}$$

where $\boldsymbol{\sigma}$ and $\boldsymbol{\varepsilon}$ are the stress and the strain tensor of the viscous matrix; and $\boldsymbol{C}_{ijkl}^{VE}$ is the time-dependent constitutive matrix showing the relaxation effect. The constitutive matrix is expressed in terms of the bulk modulus $k_m(t)$ and the shear relaxation modulus $\mu_m(t)$ as

$$\boldsymbol{C}_{ijkl}^{VE} = \left[k_m(t) - \frac{2}{3}\mu_m(t)\right]\delta_{ij}\delta_{kl} + \mu_m(t)(\delta_{ik}\delta_{jl} + \delta_{il}\delta_{jk}) \tag{20}$$

The shear relaxation modulus of the matrix is expressed as

$$\mu_m(t) = \mu_\infty + \sum_{i=1}^{n} \mu_i exp(-\frac{t}{\tau_i}) \tag{21}$$

where μ_∞ is the shear modulus of the equilibrium branch; μ_i and τ_i are the shear modulus of the non-equilibrium branches and the relaxation time, respectively. In this research, the bulk modulus $k_m(t)$ is assumed to be constant over time since many experimental results show that the matrix's shear relaxation modulus is dominant (Zhao *et al.* 2019). Consequently, it is assumed $k_m(t) = E/3(1-2v)$. According to Eq. (18), multi-phase viscoelastic particulate composite has the effective constitutive matrix given as follows

$$\boldsymbol{C}^{MT\,eff} = v_0\boldsymbol{C}^{VE}:\boldsymbol{B}^0 + \sum_{I=1}^{N} v_I\,\boldsymbol{C}^I:\boldsymbol{B}^I = \left(v_0\boldsymbol{C}^{VE} + \sum_{I=1}^{N} v_I\,\boldsymbol{C}^I:\boldsymbol{b}^I\right):\boldsymbol{B}^0 \tag{22}$$

where $\boldsymbol{B}^0$ and $\boldsymbol{B}^I$ are the global strain concentration tensors for the matrix phase and particles, respectively. The second equality in Eq. (22) is established with Eq. (13), and the relationship $\boldsymbol{B}^0 = <\boldsymbol{b}^I>^{-1}$. Here, we consider the interphase region effect. The macroscopic strain that considers the interfacial effect is proposed by Qu (1993). It is given as:

$$\boldsymbol{\varepsilon}_{macro} = \sum_{I=0}^{N} v_I\boldsymbol{\varepsilon}^I + \sum_{I=1}^{N} v_I\boldsymbol{H}^I:\boldsymbol{C}^I:\boldsymbol{\varepsilon}^I \tag{23}$$

Where $\boldsymbol{H}^I$ is the fourth-order tensor that contains the interfacial properties. As shown in Fig. 2, a spring element is utilized to reflect the imperfectly bonded interphase behavior (Qu 1993). Here, α and β are the compliances in the tangential and normal directions on the interphase, respectively.

The modified Eshelby tensor can be formulated for imperfectly bonded interfacial behavior as follows

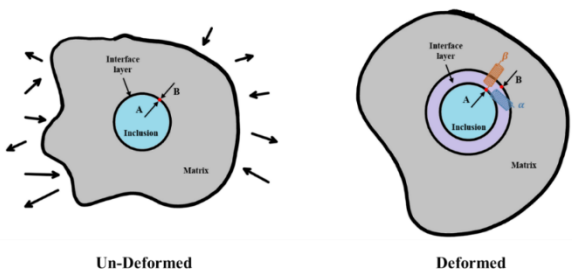

Fig. 2 Imperfectly bonded interfacial behavior of sphere inclusions

$$\boldsymbol{S}^M = \boldsymbol{S} + (\boldsymbol{I}^{tensor} - \boldsymbol{S}) : \boldsymbol{H} : \boldsymbol{C}^0 : (\boldsymbol{I}^{tensor} - \boldsymbol{S}) \tag{24}$$

For spherical inclusions, $\boldsymbol{H}$ can be represented with fourth-order tensor $\boldsymbol{P}$ and $\boldsymbol{Q}$ with interphase layer compliance parameters α and β as follows

$$\begin{gathered} \boldsymbol{H} = \alpha \boldsymbol{P} + (\beta - \alpha)\boldsymbol{Q} \\ P_{ijkl} = \frac{1}{a} I^{tensor}_{ijkl}, \qquad Q_{ijkl} = \frac{1}{5a}(2I^{tensor}_{ijkl} + \delta_{ij}\delta_{kl}) \end{gathered} \tag{25}$$

In this equation, a denotes the radius of the spherical inclusions. On the other hand, the average strain within the inclusions by applying the Mori-Tanaka scheme can be represented as

$$\boldsymbol{\varepsilon}^I = \boldsymbol{b}^I : \boldsymbol{\varepsilon}^o \tag{26}$$

The local strain concentration tensor with one-site approximation assumed is given as

$$\boldsymbol{b}^I = [\boldsymbol{I}^{tensor} + \boldsymbol{S}^M : (\boldsymbol{C}^0)^{-1} : (\boldsymbol{C}^I - \boldsymbol{C}^0)]^{-1} \tag{27}$$

Substituting Eq. (26) into Eq. (23), the macroscopic strain is expressed as

$$\boldsymbol{\varepsilon}_{macro} = \left[\sum_{I=0}^{N} v_I \, \boldsymbol{b}^I + \sum_{I=1}^{N} v_I \, \boldsymbol{H}^I : \boldsymbol{C}^I : \boldsymbol{b}^I\right] : \boldsymbol{\varepsilon}^o \tag{28}$$

$$\boldsymbol{\varepsilon}^o = \left[\sum_{I=0}^{N} v_I \, \boldsymbol{b}^I + \sum_{I=1}^{N} v_I \, \boldsymbol{H}^I : \boldsymbol{C}^I : \boldsymbol{b}^I\right]^{-1} : \boldsymbol{\varepsilon}_{macro} \tag{29}$$

Comparing Eq. (29) with Eq. (22), the global strain concentration tensor ($\boldsymbol{B}^0$) for the matrix is given as

$$\boldsymbol{B}^o = \left[\sum_{I=0}^{N} v_I \, \boldsymbol{b}^I + \sum_{I=1}^{N} v_I \, \boldsymbol{H}^I : \boldsymbol{C}^I : \boldsymbol{b}^I\right]^{-1} \tag{30}$$

Substituting Eq. (30) into Eq. (22), the modified viscoelastic effective stiffness of the particulate composite is expressed as follows

$$\begin{gathered} \boldsymbol{C}^{MT\,eff}_{ijkl} = \left[v_0 \boldsymbol{C}^{VE} + \sum_{I=1}^{N} v_I \, \boldsymbol{C}^I : \boldsymbol{b}^I\right] : \\ \left[\sum_{I=0}^{N} v_I \, \boldsymbol{b}^I + \sum_{I=1}^{N} v_I \, \boldsymbol{H}^I : \boldsymbol{C}^I : \boldsymbol{b}^I\right]^{-1} \end{gathered} \tag{31}$$

For the two-phase particulate composite, Eq. (31) can be written as

$$\begin{gathered} \boldsymbol{C}^{MT\,eff}_{ijkl} = \left[(1 - v_f)\boldsymbol{C}^{VE} + v_f \boldsymbol{C}^f : \boldsymbol{b}^f\right] : \\ \left[(1 - v_f)\boldsymbol{I}^{tensor} + v_f (\boldsymbol{I} + \boldsymbol{H}^f : \boldsymbol{C}^f) : \boldsymbol{b}^f\right]^{-1} \end{gathered} \tag{32}$$

It is also worth noting that the mean-field homogenization such as the Mori-Tanaka approach considers stress-strain fields are homogeneous per phase, which allows using of average values of each phase instead of the local values at each point. Such approximation might cause a difference in estimated volumetric stress since the actual stress-strain fields are non-uniform for phases, especially

on the matrix domain. Because of the above limitations, the isotropization technique and incremental Mori-Tanaka schemes have been developed and utilized in previous research (Doghri and Ouaar 2003, Vieville *et al.* 2006, Tchalla *et al.* 2015). However, there is a literature report that isotropization seems not to improve the accuracy of visco-platic model's predictions compared to the anisotropic model due to local concentration and anisotropic material characteristics of composites (Czarnota *et al.* 2015). Therefore, it should be selected with care. The isotropization can also be applied for the linear isotropic problem, in which case the result is the same as not applying the isotropization technique.

Analytical representation of Eshelby tensor S is only available if the Inclusion is an ellipse and the matrix material is isotropic or transversely isotropic. Therefore, in the case of matrix material is anisotropic, Eshelby tensor S can directly be computed using the stiffness of matrix (Doghri and Ouaar 2003, Vieville *et al.* 2006). This Incremental Mircromechanical Scheme (IMS) results in stiffer prediction for the mechanical behavior of composites. The isotropic part of the tangent stiffness matrix is given as

$$C^{iso} = 3K\boldsymbol{I}^{vol} + 2G\boldsymbol{I}^{dev} \tag{33}$$

Here, K and G are bulk moduli and shear modulus, respectively. $\boldsymbol{I}^{vol}$ and $\boldsymbol{I}^{dev}$ are the volumetric part and deviatoric part of the fourth-order identity tensor. We have adopted this methodology in the proposed model. However, the effect of the IMS was not significant compared to the Mori-Tanaka method.

In this research, we are proposing the novel stress prediction methodology utilizing the above homogenization methodology. The homogenized constitutive matrix is obtained for every time increment. In the case of strain input boundary conditions, the macro strain is also a known value. Therefore, the strain rate $\frac{\partial \boldsymbol{\varepsilon}_{kl}^{macro}(s)}{\partial s}$ for every time step is also known value. In this research, the stress prediction of the viscous composite is obtained by computing

$$\boldsymbol{\sigma}_{ij}(t) = \int_0^t \boldsymbol{C}_{ijkl}^{MT\ eff}(t-s) : \frac{\partial \boldsymbol{\varepsilon}_{kl}^{macro}(s)}{\partial s} ds \tag{34}$$

This stress prediction methodology is intuitive and straightforward. However, to the best knowledge of authors, there has been no study on the viscoelastic composite material's stress prediction with this methodology. Therefore, this methodology is proposed with both numerical and experimental verifications. The verification results are presented in Section 3.

2.3 Numerical implementation of the micromechanical model

Fig. 3 shows a flowchart of the proposed algorithm. For every increment, the local and global strain concentration tensors are iteratively updated by constantly changing tangent constitutive stiffness matrices of the particle and the matrix. Viscoelasticity is applied to only the matrix, and the particle is assumed to be linear elastic. After the strain concentration tensors are computed, the effective constitutive matrix and effective stress of the composite material are computed.

Detailed numerical procedures for the proposed method are summarized in Table 1. The numerical procedures are shown by presenting the case that the interphase area effect and IMS are considered. For a time $[t_n,\ t_{n+1}]$ increment, the input variables are: the macro strain $\boldsymbol{\varepsilon}_{macro}^{r}(t_n)$ at time step t_n and the macro strain increment $\Delta\boldsymbol{\varepsilon}_{macro}^{r}$ such as $\boldsymbol{\varepsilon}_{macro}^{r}(t_{n+1}) = \boldsymbol{\varepsilon}_{macro}^{r}(t_n) + \Delta\boldsymbol{\varepsilon}_{macro}^{r}$. The output variable is the effective stress of the composites. The effective stress is

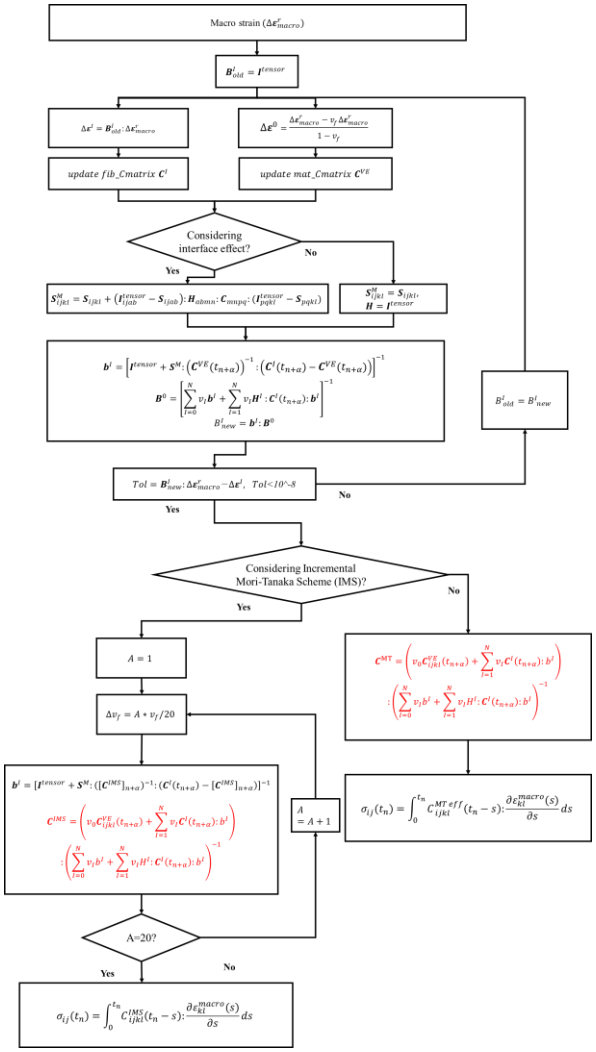

Fig. 3 Flowchart of the proposed algorithm for viscoelastic particulate composites

calculated by Boltzmann integrating the incremental value of the $\boldsymbol{C}^{IMS\,eff}_{ijkl}(t_n - s)$ and $\frac{\partial \boldsymbol{\varepsilon}^{macro}_{kl}(s)}{\partial s}$ over time. Assuming that Δt_i is small enough, the strain rate at time t_i value $\frac{\partial \boldsymbol{\varepsilon}^{macro}_{kl}}{\partial s}(t_i)$ is calculated as

$$\frac{\partial \boldsymbol{\varepsilon}^{macro}_{kl}}{\partial s}(t_i) \approx \frac{\boldsymbol{\varepsilon}^{macro}_{kl}(t_i) - \boldsymbol{\varepsilon}^{macro}_{kl}(t_{i-1})}{\Delta t_i} = \frac{\Delta \boldsymbol{\varepsilon}^{macro}_{kl}(t_i)}{\Delta t_i} \tag{35}$$

Combining Eqs. (34) and (35), the effective stress at time t_n can be represented as

$$\boldsymbol{\sigma}_{ij}(t_n) = \sum_{i=1}^{n} \boldsymbol{C}^{IMS\,eff}_{ijkl}(t_n - t_i) \frac{\Delta \boldsymbol{\varepsilon}^{macro}_{kl}(t_i)}{\Delta t_i} \Delta t_i \tag{36}$$

Table 1 Pseudocodes for the proposed homogenization method

Numerical implementation
1. Compute the strain increment in the inclusions: $\Delta\boldsymbol{\varepsilon}^I = \boldsymbol{B}^I \Delta\boldsymbol{\varepsilon}^r_{macro}$
2. Compute the constitutive matrix of the matrix: $\boldsymbol{C}^{VE}_{ijkl}(t_n) = \left[k_m(t_n) - \frac{2}{3}\mu_m(t_n)\right]\delta_{ij}\delta_{kl} + \mu_m(t_n)(\delta_{ik}\delta_{jl} + \delta_{il}\delta_{jk})$
3. Compute the strain increment in the matrix: $\Delta\boldsymbol{\varepsilon}^0 = \frac{\Delta\boldsymbol{\varepsilon}^0_{macro} - v_I \Delta\boldsymbol{\varepsilon}^I}{1 - v_I}$
4. Update the algorithmic constitutive matrix of matrix: $\boldsymbol{C}^{VE}_{ijkl}(t_{n+1})$
5. Apply the mid-point ($\alpha = 0.5$) rule at the time $t_{n+\alpha}$ for obtaining the algorithmic constitutive matrix: $\boldsymbol{C}^{VE}_{ijkl}(t_{n+\alpha}) = (1-\alpha)\boldsymbol{C}^{VE}_{ijkl}(t_n) + \alpha\boldsymbol{C}^{VE}_{ijkl}(t_{n+1})$
6. Compute the global strain concentration tensor: $\boldsymbol{B}^I = \boldsymbol{b}^I : \boldsymbol{B}^0$
7. Calculate the residual to determine the compatibility of the mean strain in the inclusion phase: $R = \boldsymbol{B}^I \Delta\boldsymbol{\varepsilon}^r_{macro} - \Delta\boldsymbol{\varepsilon}^I$
8. If $\lvert R\rvert \le TOL$, exit the loop and go to step 10
9. If not $\lvert R\rvert \le TOL$, go to step 1 for the new iteration using the computed $\boldsymbol{B}^I$
10. Volume fraction increment $A=1$
11. Compute volume increment: $\Delta v_f = A * v_f/20$
12. Compute constitutive matrix of composites and save: $\boldsymbol{C}^{IMS} = \left(v_0\boldsymbol{C}^{VE}_{ijkl}(t_{n+\alpha}) + \sum_{I=1}^{N} v_I \boldsymbol{C}^I(t_{n+\alpha}) : b^I\right)\left(\sum_{I=0}^{N} v_I b^I + \sum_{I=1}^{N} v_I H^I : \boldsymbol{C}^I(t_{n+\alpha}) : b^I\right)^{-1}$
13. If $A = 20$, exit the loop and go to step 15
14. If $A \neq 20$, update A and go to step 11
15. Compute the effective stress of the composites: $\boldsymbol{\sigma}_{ij}(t_n) = \sum_{i=1}^{n} \boldsymbol{C}^{IMS\,eff}_{ijkl}(t_n - t_i)\frac{\Delta\boldsymbol{\varepsilon}^{macro}_{kl}(t_i)}{\Delta t_i}\Delta t_i$

For instance, in the particular case of given strain input $\boldsymbol{\varepsilon}^{macro}_{kl}(s) = A_{kl}\sin(2\pi f s)$ where A_{kl} is a constant matrix for strain magnitude, the $\frac{\partial\boldsymbol{\varepsilon}^{macro}_{kl}(s)}{\partial s}$ value is obtained as $2\pi f A_{kl}\cos(2\pi f s)$. Therefore, the stress can be predicted by using Eq. (34) as

$$\boldsymbol{\sigma}_{ij}(t_n) = \sum_{i=1}^{n} \boldsymbol{C}^{IMS\,eff}_{ijkl}(t_n - t_i) 2\pi f \cos(2\pi f t_i)\,\Delta t_i \tag{37}$$

For general strain input histories, $\frac{\partial\boldsymbol{\varepsilon}^{macro}_{kl}(s)}{\partial s}$ can be calculated numerically and the stress can be obtained by summation of $\boldsymbol{C}^{MT\,eff}_{ijkl}(t_n - s)\frac{\partial\boldsymbol{\varepsilon}^{macro}_{kl}(s)}{\partial s}$. In Eq. (37), time delaying effect and relaxation effect is shown by calculating the stress by Boltzmann integrating the multiplication of the tangent stiffness and the strain rate. This stress prediction methodology formulated in this paper was implemented as an ABAQUS UMAT to solve large scale problems with a commercial finite element solver. The implementation of the ABAQUS UMAT provides benefits 1) to control effects of the volume fraction, imperfect interphase layer and inclusion stiffness and 2) to use the viscoelastic model for the pure resin calibrated with experimental relaxation test.

3. Numerical verification

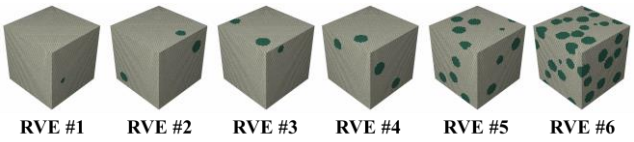

(a) DNS FE models without an interphase layer

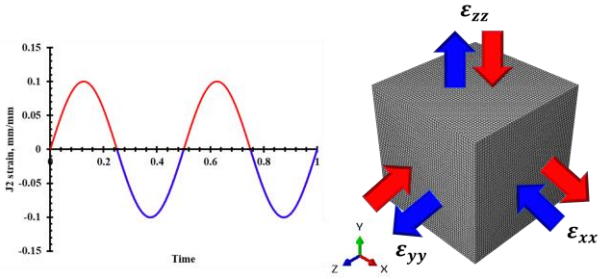

(b) cyclic normal loading & PBC

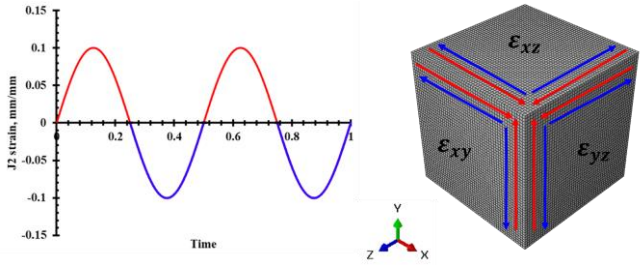

(c) cyclic shear loading & PBC

Fig. 4 FE model and Load & boundary condition for DNS model

In this section, the proposed homogenization model is verified with FE based DNS results in dynamic mechanical responses. Six representative volume finite element models are generated using commercial software, DIGIMAT (Digimat 2011), and DNS is performed with ABAQUS.

3.1 Direct numerical simulation

The RVE DNS model was meshed with voxels. Total 125,000 elements ($50 \times 50 \times 50$) are used for the DNS models. The dimension of the model is $1\ \text{mm} \times 1\ \text{mm} \times 1\ \text{mm}$. Element type C3D8 with full integration method is used considering the unidirectional loading condition without bending. The two kinds of FE models have generated: 1) models without interphase layer 2) models with an interphase layer. Fig. 4(a) shows the FE models without an interphase layer. The volume fractions of the RVE#1 to RVE#6 are 1%, 2%, 3%, 5%, 10%, and 20%, respectively. Fig. 4 (b) and (c) shows the given uniaxial and shear boundary condition for the FE models. The periodic boundary condition is applied. Although the periodic boundary condition is not clearly seen in Fig. 4, it is applied with constraints equation in the ABAQUS input files.

Fig. 5 shows the geometry and a FE model with an interphase layer. The interphase thickness is assumed to be 15% of the particle radius.

For the DNS model's material properties, the elastic material properties are applied to the particle phase, and the viscoelastic material properties are applied to the matrix phase. The generalized

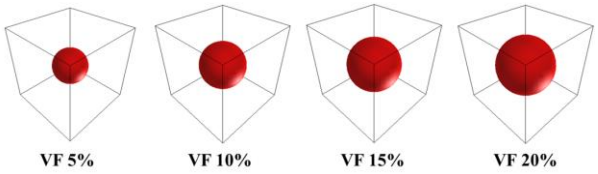

(a) Geometry of the DNS model

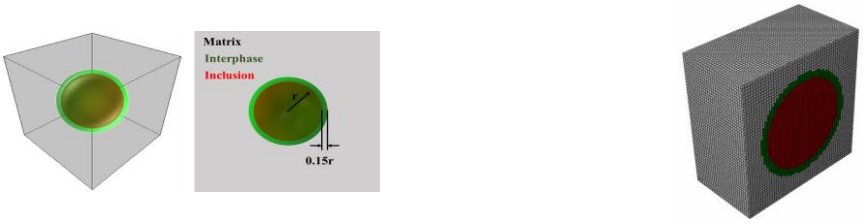

(b) Interphase layer modeling (c) FE model (VF 15%)

Fig. 5 DNS FE models with an interphase layer

Table 2 Material parameters for DNS model and homogenization model

Particle		Matrix							
E (MPa)	ν	E (MPa)	ν	E_1 (MPa)	E_2 (MPa)	E_3 (MPa)	τ_1 (s)	τ_2 (s)	τ_3 (s)
100	0.22	0.195	0.497	0.351	1.75	0.186	0.442s	0.0084s	0.218s

Maxwell model with one spring and three Maxwell elements is used for the viscoelastic material parameters. Table 2 shows the material parameters used for the FE analysis and material parameters used for the homogenization model's matrix and inclusion constitutive matrix. For the homogenization model, the volume fraction of the RVE is also given as material input data. Here, E is young's modulus, ν is the Poisson's ratio and $E_1, E_2, E_3, \tau_1, \tau_2, \tau_3$ are the Generalized Maxwell Model parameters. The viscoelastic material properties are obtained from the literature (Gillani 2018). The viscoelastic material parameters are obtained from the literature to make it objective and the materials parameters for the particle is assumed to be almost 50 times stiffer compared to the matrix phase. In this paper, Young's modulus of the interphase model is assumed to be 1% of Young's modulus of the particle.

The periodic boundary condition is applied for the loading boundary condition. The sinusoidal strain loading is applied with normal macro strains ($\boldsymbol{\varepsilon}_{ij}^{macro}$) as follows

$$\boldsymbol{\varepsilon}_{ij}^{macro} = \begin{bmatrix} 0.1 & 0 & 0 \\ 0 & -0.05 & 0 \\ 0 & 0 & -0.05 \end{bmatrix} sin(2\pi ft) \tag{38}$$

The shear loading condition is also applied with pure shear macro strains ($\boldsymbol{\varepsilon}_{ij}^{macro}$) as follows

$$\boldsymbol{\varepsilon}_{ij}^{macro} = \begin{bmatrix} 0 & 0.05 & 0.05 \\ 0.05 & 0 & 0.05 \\ 0.05 & 0.05 & 0 \end{bmatrix} sin(2\pi ft) \tag{39}$$

Here, f is the loading frequency of the sinusoidal loading. For DNS, the loading frequency of 2 Hz is applied considering the computing time of the DNS. Total 50 volume-averaged stress and strain datasets are obtained from the DNS. The total time is assumed to be 1 second, and datasets

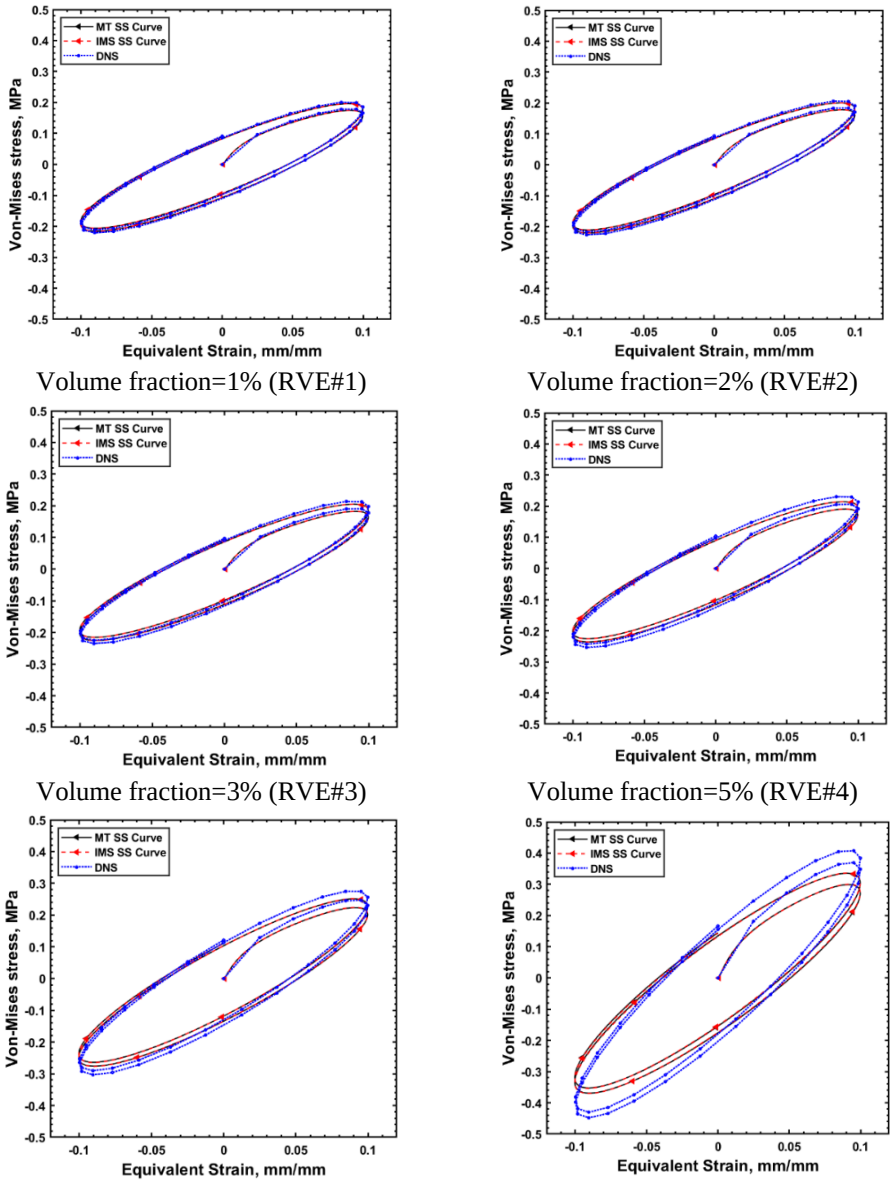

Volume fraction=1% (RVE#1) Volume fraction=2% (RVE#2)

Volume fraction=3% (RVE#3) Volume fraction=5% (RVE#4)

Volume fraction=10% (RVE#5) Volume fraction=20% (RVE#6)

Fig. 6 Comparisons of the effective bulk stress-strain hysteresis curves for the DNS and the proposed homogenization models

are obtained every 0.02 seconds.

3.2 Verification results without ınterphase layer

3.2.1 Stress-strain hysteresis curve

Stress-strain hysteresis curves of composites with different volume fractions are examined to

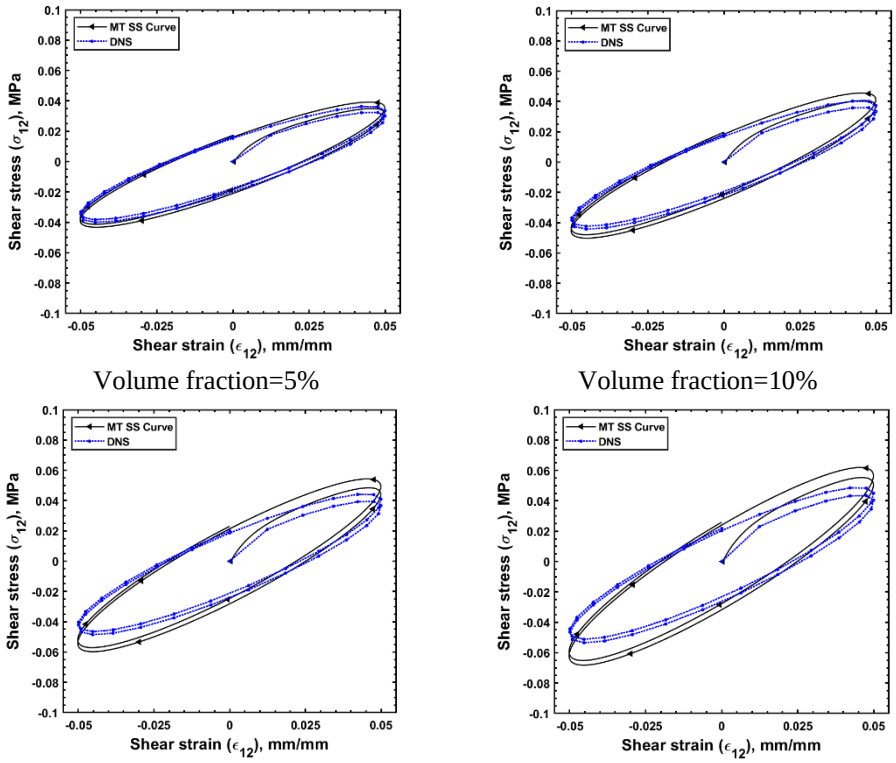

Fig. 7 Comparisons of the effective stress-strain hysteresis curves for the DNS and the proposed homogenization model

verify the proposed model. The effective bulk response from the homogenization model is compared by the DNS models in Fig. 4(a) subjected to the uniaxial loading condition of Eq. (38). Fig. 6 shows comparisons of the von-Mises stress $(\sigma_{von} = \sqrt{3J_2} = \frac{1}{2} * [(\sigma_{11} - \sigma_{22})^2 + (\sigma_{22} - \sigma_{33})^2 + (\sigma_{33} - \sigma_{11})^2 + 6 * (\sigma_{23}^2 + \sigma_{31}^2 + \sigma_{12}^2)]))$ and equivalent strain $(\varepsilon_{eq} = \sqrt{\frac{2}{3}\varepsilon_{ij}^{dev} : \varepsilon_{ij}^{dev}})$ hysteresis curves for the proposed model and DNS model.

The effective shear response is also compared to verify the homogenization model. The DNS models in Fig. 5(a) with no interphase layer are used under the pure shear loading condition in Eq. (39). Because the RVE models have a symmetric geometry, the shear stresses $(\sigma_{12}, \sigma_{13}, \sigma_{23})$ are identical to each other. Fig. 7 shows comparisons of the stress (σ_{12})-strain (ε_{12}) hysteresis curves for the proposed homogenization model and DNS model.

The shape of the stress-strain hysteresis curve was ellipsoidal representing the viscoelasticity of the material. As the volume fraction increases, the stress amplitude and stiffness of hysteresis curves are varied. The proposed homogenization model results showed well matching prediction considering that the Mori-Tanaka model generally has a limitation in the accuracy of the global stress-strain response at relatively high-volume fractions. For the 20% volume fraction, the proposed model appeared to underestimate the bulk stiffness but overestimate the shear stiffness. This discrepancy is caused by assumptions of homogeneous stress and strain fields in the Eshelby

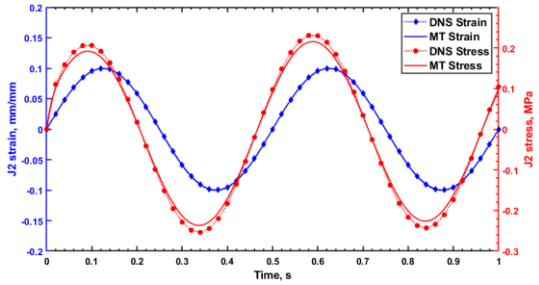

(a) Stress and strain curves in the time domain

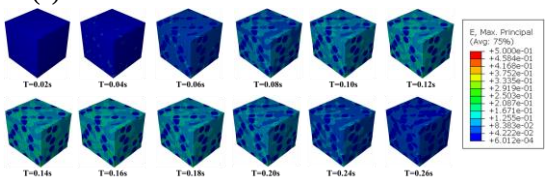

(b) time-varying strain contours

Fig. 8 Numerical simulation of DNS model

inclusion theory-based micromechanics model while actual stress and strain fields are heterogeneous. To improve the accuracy of the stress prediction by the proposed homogenization scheme, we have also tried the Mori-Tanaka model with IMS. However, the effects of the IMS on the stress prediction were negligible.

3.2.2 Stress and strain responses in time domain

The time-varying stress and strain responses are examined for the proposed homogenization model and DNS model. Fig. 8(a) shows the stress and strain curves in the time-domain at a volume fraction of 5% with normal strain loading condition. Fig. 8(b) shows the time-varying strain contours of the DNS model. According to the load and boundary condition, the proposed model's strain shows exact sinusoidal behavior while the stress of the DNS model and homogenization model shows the response delay and stress relaxation effect. The result shows that the prediction of the homogenization model is reasonable and consistent with the DNS results.

3.2.3 Prediction of dynamic mechanical property

The tangent delta (Tan δ) is an important index for viscoelastic materials. The periodic sinusoidal strain loading condition generates sinusoidal periodic stress with a different phase due to the time delay characteristics of the viscoelastic material properties. This creates a phase shift (δ) between the applied strain and resulted stress. The dynamic mechanical properties are defined using this phase shift and expressed as follows

$$E' = \frac{\sigma_0}{\varepsilon_0}\cos(\delta), \qquad E'' = \frac{\sigma_0}{\varepsilon_0}\sin(\delta), \qquad \text{Tan}\,\delta = \frac{\sigma_0}{\varepsilon_0}\cos(\delta) \tag{40}$$

$$\text{Where } \varepsilon = \varepsilon_0 \sin(wt) \text{ and } \sigma = \sigma_0 \sin(wt + \delta)$$

Here, E', E'', and Tan δ are the storage modulus, loss modulus and tangent delta of the viscoelastic material. Fig. 9 shows the tangent delta results of the DNS and the proposed homogenization model in the frequency domain. The pure matrix response is provided for

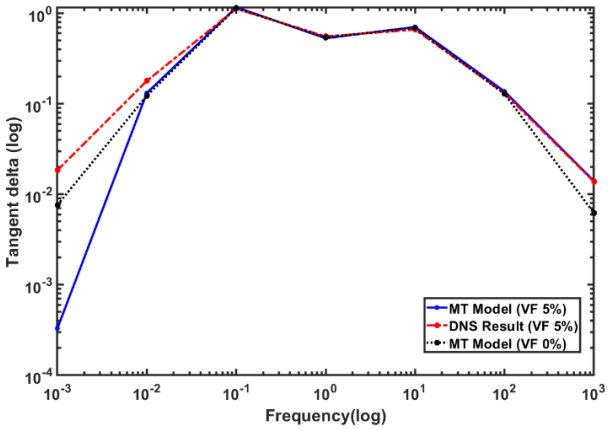

Fig. 9 $\tan(\delta)$ prediction results according to the loading frequency (V_f: 5 %)

comparison. In particular, there is a major deviation of tangent delta between the MT model (VF 5%) and MT model (VF 0%), especially at low and high frequencies. This deviation is caused by varying viscoelastic characteristics according to the composite's volume fraction. At low frequency, the viscosity of the system is larger if volume fraction is lower and therefore, the tangent delta of MT model (VF 0%) is higher. However, at high frequency, the tangent delta of the MT model (VF 5%) is higher since the rubbery phase and plastic phase varies according to the frequency (Khan *et al.* 2005). The tangent delta values showed a peak in the frequency on the 0.1 Hz, which is well-known behavior of the viscous material. The peak of the $\mathrm{Tan}\,\delta$ exhibits because the ratio of the elastic response to viscous response changes as the loading frequency changes. The deviation of tangent delta between the MT model (VF 5%) and DNS result (VF 5%) at low frequencies can be explained by the relaxation of viscoelastic material. When the frequency is extremely low, the constitutive matrix of viscoelastic material relaxes largely between step increments since the time increment is large, resulting such a deviation. The loss modulus is low at the low-temperature glass state because of the slow molecules' mobility. Therefore, as the temperature increases, the $Tan\,\delta$ value increases toward a peak value. However, as the material state enters into a rubbery state at the high temperature, the $\mathrm{Tan}\,\delta$ value decreases again because the molecules are physically entangled. For this reason, the $\mathrm{Tan}\,\delta$ value has a peak value at a certain frequency considering the time-temperature superposition principle. The tangent delta results by the proposed model are also well matched with the data from the DNS.

3.3 Verification results with ınterphase layer

The verification of the proposed homogenization model with the interphase layer is also conducted. Four FE models are generated. According to the literature (Qu 1993), $\boldsymbol{\alpha}$ and $\boldsymbol{\beta}$ in Eq. (25) can be calculated with material properties of the interphase layer as follows

$$\alpha = \frac{t}{\mu_i}, \qquad \beta = \frac{t}{(K_i + \frac{4\mu_i}{3})} \tag{41}$$

Here, t is the interphase thickness, and μ_i and K_i are the shear and bulk moduli of the interphase layer, respectively. Stress-strain hysteresis curves of composites with the interphase layer

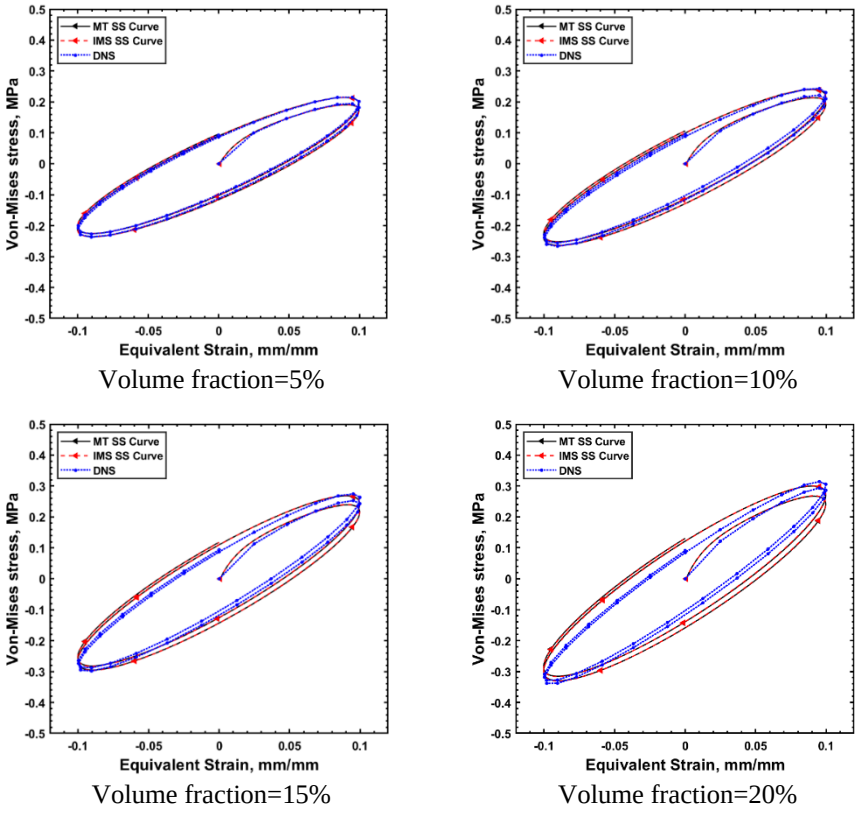

Fig. 10 Stress-strain hysteresis curve considering the interphase layer

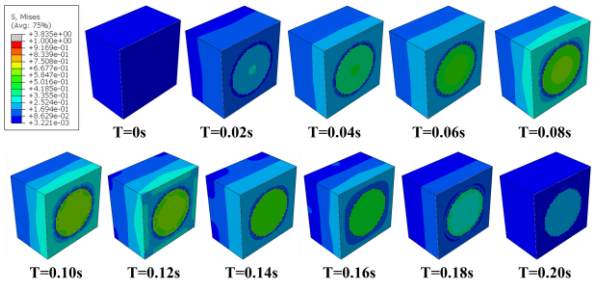

Fig. 11 DNS stress results according to the time (V_f: 15 %)

are examined to verify the proposed homogenization model. Fig. 10 shows comparisons of the proposed homogenization model and DNS results. The proposed homogenization model's stress prediction with the interphase layer showed a better matching tendency with DNS results than the model without an interphase layer for the 20% high-volume fraction. Since the predicted stress values of the Mori-Tanaka model have the same value for DNS model that have same volume fraction and the same shape regardless of the number of particles, the accuracy of the two models is compared. This result shows that modeling the appropriate interphase layer can improve the proposed homogenization method's accuracy versus corresponding DNS model.

Fig. 11 shows the DNS stress results over the time increments. The results show that the stress is concentrated on the particle phase. Although strain contours were not provided, the strain in the interphase layer and matrix phase was much larger than that of the particle phase.

4. Experimental verification

To experimentally verify the proposed homogenization model, experiments with DMA equipment were conducted. After presenting the experimental specimen, equipment, materials properties, and dynamic mechanical analysis results, the proposed homogenization method model's numerical results are compared with experimental results.

4.1 Materials and Equipment for DMA test

Four types of specimens are fabricated with silicone and glass beads for DMA tests of particulate composites. The silicone is a viscous matrix and the glass beads are elastic reinforcements. The silicone used in the experiment is a SORTA-Clear 40™ Smooth-On, Inc® and the glass beads used in the experiment are spherical-shaped high-purity grade silica (SiO_2) with 75 micrometers from the Supelco® Sigma-Aldrich®. Particulate composites with volume fractions of 0%, 5%, 10%, and 20% are fabricated for the DMA. The silicone and glass beads were mechanically mixed for five minutes and degassed using a Lab1st® vacuum chamber at -99.28 kPa for seven minutes. After degassing, the composite was poured into cuboid-shaped molds and cured for 24 hours. The physical dimensions of the cuboid are 10 mm×10 mm×4 mm. Total ten specimens with the same volume fraction ratio are fabricated. Fig. 12 shows the schematics of specimen samples and the equipment used for the experiments. For the dynamic mechanical analysis, DMA/SDTA861e from the Mettler Toledo AG® is utilized.

4.2 Materials and equipment for relaxation test

The material properties of the glass bead and matrix are obtained from the literature and relaxation test, respectively. Table 3 shows the material properties of the glass bead and matrix. In the case of the glass beads' properties, it is presented as a range and the intermediate values were used in the simulation. The relaxation test is conducted to obtain the viscoelastic material properties for the matrix (SORTA-Clear 40™ Smooth-On, Inc®). The cylindrical shape samples with a

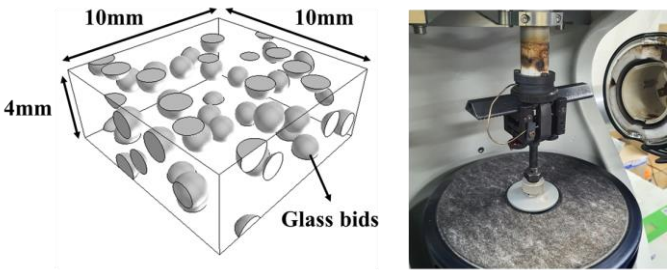

Fig. 12 The schematics of specimen samples and experimental equipment for DMA

Table 3 Particle and matrix properties: values in the parentheses are used for the simulation

Parameter	Value	Unit
$E_{particle}$	66.3 – 74.8 (70)	GPa
$\nu_{particle}$	0.15 – 0.19 (0.17)	-
E_{matrix}	24.99	MPa
ν_{matrix}	0.45	-

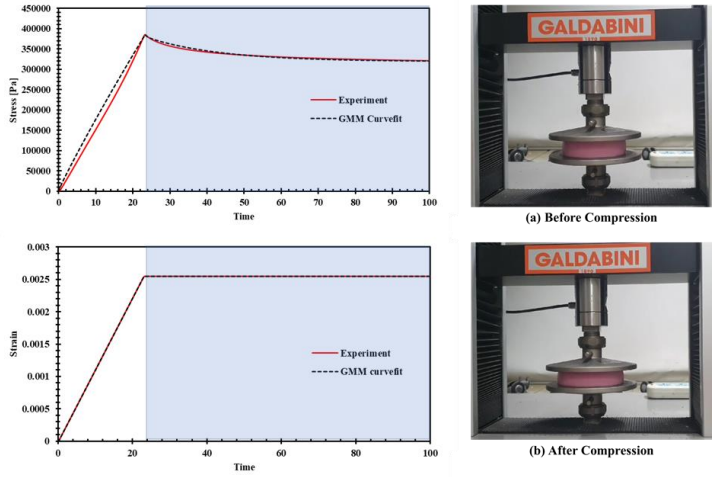

Fig. 13 Stress & strain according to the time and specimen & equipment

Table 4 Generalized maxwell parameters of the matrix

i	$\tau_i(s)$	W_i(Mpa)
1	0.2300	8.6154
2	20.0	13.498
3	0.2865	8.7361
4	0.3980	8.4561
5	1.0780	7.8483

diameter of 10 cm and a thickness of 3 cm are used for the relaxation test. Fig. 13 shows the stress, strain over time, specimens, and testing equipment. A UTS (Universal Testing Machine) machine, Quasr 25 (GALDABINI, Inc®), is used for the relaxation test.

Generalized Maxwell parameters are obtained by curve fitting the relaxation test results as a prony series with an optimization method in the literature (Babaei *et al.* 2016). Table 4 shows the obtained Generalized Maxwell parameters for the matrix (SORTA-Clear 40™ Smooth-On, Inc®).

4.3 Experimental results of the dynamic mechanic analysis

The dynamic mechanical analysis is performed for the specimen with volume fractions 0%, 5%, 10%, and 20%. From DMA tests, the tangent delta, loss modulus, and specimens' storage modulus were evaluated. Fig. 14 shows the tangent delta, loss modulus, and storage modulus of specimens according to the loading frequency. The experimental data were obtained by averaging the

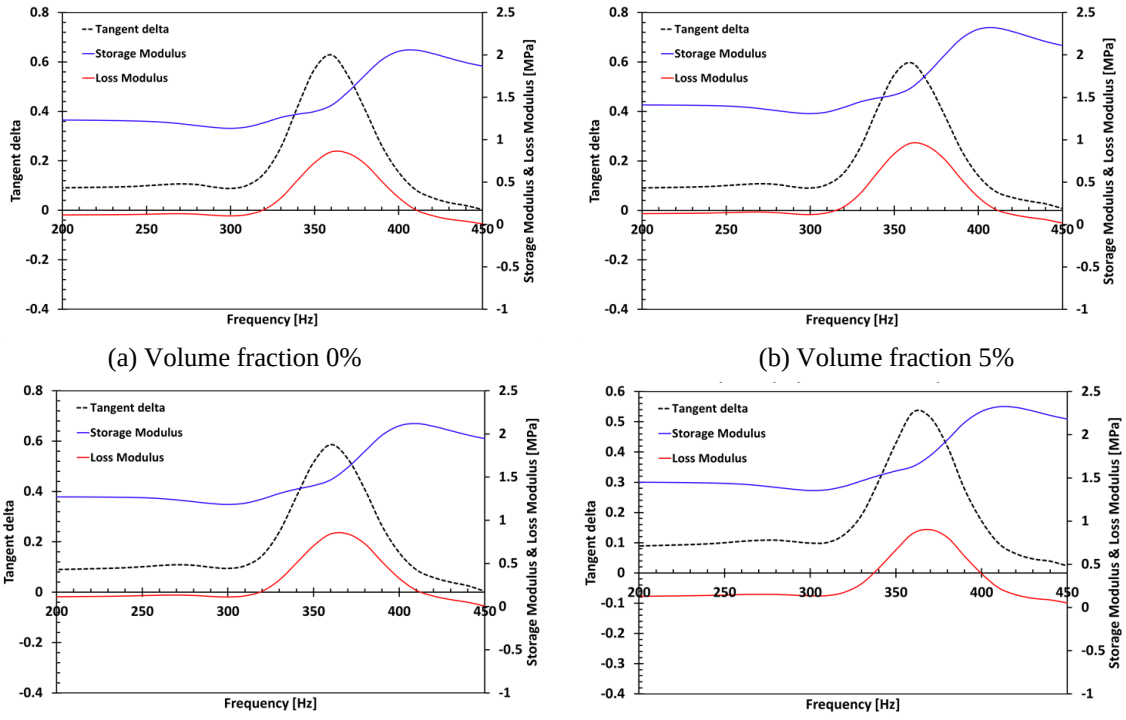

(a) Volume fraction 0%

(b) Volume fraction 5%

(c) Volume fraction 10%

(d) Volume fraction 20%

Fig. 14 Dynamic mechanical properties of the particulate composite (The color is distinguished in the online version)

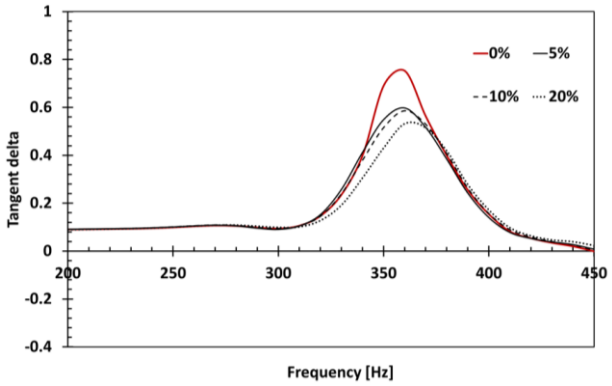

Fig. 15 Tangent delta of the particulate composite

experimental results of the five samples from each volume fraction.

Fig. 15 shows the tangent delta values according to the volume fraction of the particulate composite specimens. The larger the volume fraction is, the smaller the peak value of the tangent delta is. This observation implies that glass beads physically interfere with the molecular motions, resulting in reductions of viscosity. Moreover, the higher the volume fraction is, the later the peak value of tan delta occurs. The glass bead increases the free volume, while interacting with polymer

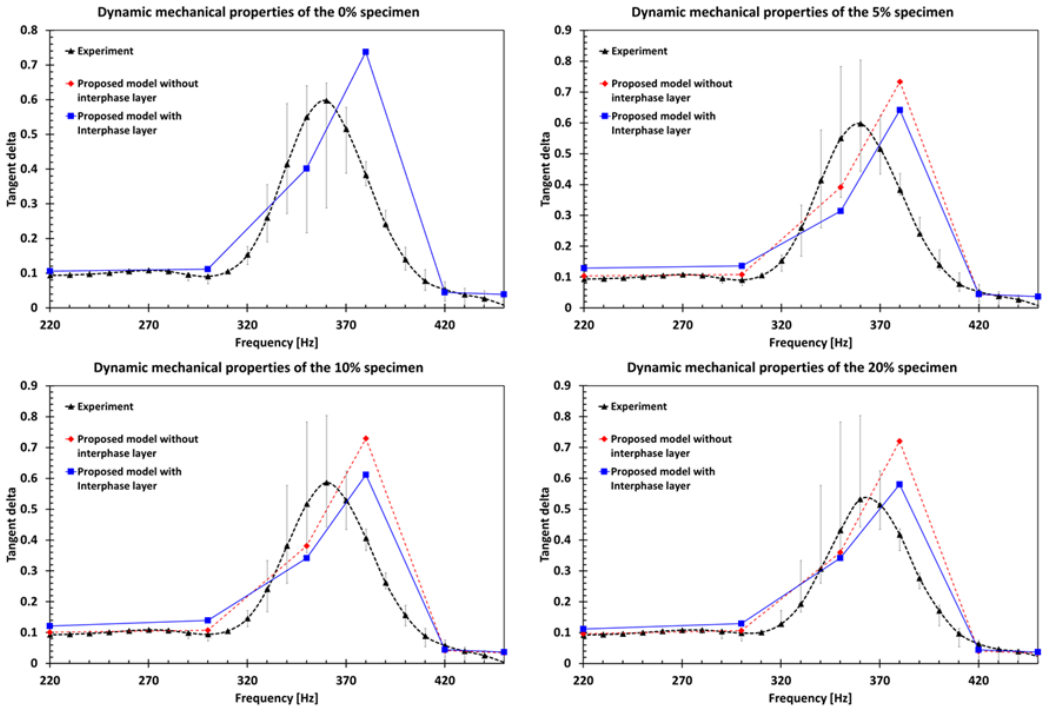

Fig. 16 Tangent delta value from the experiment and the proposed model

molecules. The free volume lowers the activation energy barrier and has a tendency of increasing molecular mobility at a relatively low temperature. Therefore, the peak of the tangent delta is shifted to the higher frequency owing to the time-temperature superposition principle. In other words, because the glass beads inhibit the polymer molecules' mobility, it requires a higher loading frequency to reach the peak tangent delta. Therefore, relaxation and retardation time decreases, resulting in the peak at a higher frequency.

4.4 Verification of the proposed model with DMA test results

The dynamic mechanical properties are predicted using the proposed homogenization method and compared with the experimental results. The tangent delta, which is the phase difference between the stress and strain, is obtained by the proposed homogenization method. The material properties shown in Table 3 and Table 4 are used as inputs for the proposed model. For the load and boundary conditions, sinusoidal strain loading according to the time is applied. Fig. 16 shows the tangent delta value obtained by the proposed method and experiment. For the experiment, five tests were conducted for each volume fraction and averaged results with an error bar representing the minimum and the maximum value is shown in Fig. 16. Tangent delta is predicted by two models: one without considering the interphase layer and one with the interphase layer. Considering the literature study that the mechanical properties of the interphase layer are higher than that of the matrix but lower than that of glass beads, it is assumed that Young's modulus of the interphase layer is 2.8 times that of the matrix. (Kitey and Tippur 2005, Müller 2017) The interphase thickness is assumed to be 15% of the particle radius. For volume fraction 0%, the tangent delta prediction was

identical since there are no particles and interphase layer. The tangent delta values from the proposed model are dependent on the applied strain rate and the total time. The comparison results show that the tendency is consistent according to the frequency. However, there are differences in the proposed model's tangent delta peak and the experimental data for volume fractions of 5%, 10%, and 20%. The tangent delta peak values' difference may be caused by the stochastic nature of material properties during the experiment and inaccurate assumptions of parameters used in the proposed model. Another possibility for the difference between tangent delta value of experiment and simulation is due to dimensional difference between DMA test obtaining tangent delta and relaxation test obtaining material properties. It is noticeable that the proposed model with the interphase layer showed closer results to the experimental results than the one without the interphase layer. By assuming the interfacial layer effect, it is possible to predict the mechanical behavior of the composite considering the debonding between the filler and matrix. However, the 2.8 times higher interphase modulus than the matrix's modulus is not an exact number obtained from the experiment but to show the consideration of the interphase layer effect can affect the simulation results.

5. Conclusions

This paper proposed a novel micromechanics-based time-domain viscoelastic constitutive model for particulate composites based on the viscoelastic constitutive model and Eshelby inclusion theory-based micromechanics model. The incremental micromechanical scheme and isotropization techniques were also applied to the proposed model to resolve the original micromechanics model's limitations. Besides, imperfect interfacial bonding was considered for better correlation with experimental test data. The proposed model is intuitive and straightforward in that the stresses are calculated from Boltzmann integral equation in terms of the homogenized viscoelastic stiffness and strain rate histories. The merits of the presented model can be summarized as follows. Unlike models based on the Laplace-Carson transformation, the proposed model does not need a cumbersome inverse Laplace-Carson transformation to obtain time-domain responses of viscous composites and can also be extended to a nonlinear viscoelastic constitutive model. In addition, the adoption of the proven homogenization technique, the Mori-Tanaka method, retained the advantage of being easily implemented in finite element codes and the ability to adapt most viscoelastic models, as presented with the generalized maxwell model.

For verifications, dynamic mechanical properties and stress responses by the proposed model were compared with those by DNS models and DMA tests. The proposed model was well verified with DMA and DNS results by comparing time-varying stress response, cyclic stress-strain curves, and tangent delta dynamic mechanical properties. The strain-stress hysteresis curves according to the volume fraction were examined and validated by the DNS. The proposed model's validation results are more reliable on a region with a relatively low volume fraction. Further investigations considering the interphase layer were also conducted. The stress prediction results considering the interphase layer showed that the proposed model shows well-matching predictions on high-volume fractions. Also, the dynamic mechanical property was examined with DNS and the proposed method. The experiment to obtain the viscous composite's dynamic mechanical properties was conducted and compared with the proposed model's prediction results. The tangent delta, an important index of viscoelastic materials, was also examined according to the loading frequency. The comparison results of the experiment and the proposed model showed a consistent tendency. The proposed model can also be extended to nonlinear viscoelastic composite materials and is useful

for multiscale analyses of viscoelastic composite materials. In addition, a constitutive model that can reflect the stochastic layout of particles is also an interesting topic that can be expanded in this study.

- Novel micromechanics-based time-domain viscoelastic constitutive model for particulate composites is proposed.
- Pseudo code and flowchart for implementation of proposed micromechanics model is presented.
- Stress response according to the volume fraction of the particulate composite is examined.
- Numerical and experimental verification of the proposed micromechanics model is presented.
- Dynamic mechanical properties of the viscous particulate composite can be predicted with proposed micromechanics model.

Acknowledgments

This work was supported by the Institute of Engineering Research of Seoul National University, and U.S. Air Force Office of Scientific Research under award number FA2386-20-1-4067. Authors are grateful for the supports.

References

Azoti, W.L., Bonfoh, N., Koutsawa, Y., Belouettar, S. and Lipinski, P. (2013), "Influence of auxeticity of reinforcements on the overall properties of viscoelastic composite materials", *Mech. Mater.*, **61**, 28-38. https://doi.org/10.1016/j.mechmat.2013.02.002.

Babaei, B., Davarian, A., Pryse, K.M., Elson, E.L. and Genin, G.M. (2016), "Efficient and optimized identification of generalized Maxwell viscoelastic relaxation spectra", *J. Mech. Behav. Biomed. Mater.*, **55**, 32-41. https://doi.org/10.1016/j.jmbbm.2015.10.008.

Berbenni, S., Dinzart, F. and Sabar, H. (2015), "A new internal variables homogenization scheme for linear viscoelastic materials based on an exact Eshelby interaction law", *Mech. Mater.*, **81**, 110-124. https://doi.org/10.1016/j.mechmat.2014.11.003.

Brenner, R., Masson, R., Castelnau, O. and Zaoui, A. (2002), "A "quasi-elastic" affine formulation for the homogenised behaviour of nonlinear viscoelastic polycrystals and composites", *Eur. J. Mech.-A/Solid.*, **21**(6), 943-960. https://doi.org/10.1016/S0997-7538(02)01247-0.

Brinson, L.C. and Lin, W. (1998), "Comparison of micromechanics methods for effective properties of multiphase viscoelastic composites", *Compos. Struct.*, **41**(3-4), 353-367. https://doi.org/10.1016/S0263-8223(98)00019-1.

Chen, Y., Yang, P., Zhou, Y., Guo, Z., Dong, L. and Busso, E.P. (2020), "A micromechanics-based constitutive model for linear viscoelastic particle-reinforced composites", *Mech. Mater.*, **140**, 103228. https://doi.org/10.1016/j.mechmat.2019.103228.

Christensen, R.M. (1969), "Viscoelastic properties of heterogeneous media", *J. Mech. Phys. Solid.*, **17**(1), 23-41. https://doi.org/10.1016/0022-5096(69)90011-8.

Czarnota, C., Kowalczyk-Gajewska, K., Salahouelhadj, A., Martiny, M. and Mercier, S. (2015), "Modeling of the cyclic behavior of elastic–viscoplastic composites by the additive tangent Mori–Tanaka approach and validation by finite element calculations", *Int. J. Solid. Struct.*, **56-57**, 96-117. https://doi.org/10.1016/j.ijsolstr.2014.12.002.

DeBotton, G. and Tevet-Deree, L. (2004), "The response of a fiber-reinforced composite with a viscoelastic matrix phase", *J. Compos. Mater.*, **38**(14), 1255-1277. https://doi.org/10.1177/0021998304042732.

Dederichs, P.H. and Zeller, R. (1973), "Variational treatment of the elastic constants of disordered materials", *Zeitschrift für Physik A Hadrons and Nuclei*, **259**(2), 103-116. https://doi.org/10.1007/BF01392841.

Digimat, A. (2011), "Software for the linear and nonlinear multi-scale modeling of heterogeneous materials", e-Xstream Engineering, Louvain-la-Neuve, Belgium.

Doghri, I. and Ouaar, A. (2003), "Homogenization of two-phase elasto-plastic composite materials and structures: Study of tangent operators, cyclic plasticity and numerical algorithms", *Int. J. Solid. Struct.*, **40**(7), 1681-1712. https://doi.org/10.1016/S0020-7683(03)00013-1.

Dunn, M.L. (1995), "Viscoelastic damping of particle and fiber reinforced composite materials", *J. Acoust. Soc. Am.*, **98**(6), 3360-3374. https://doi.org/10.1121/1.413823.

Dutra, V.F.P., Maghous, S., Campos, A. and Pacheco, A.R. (2010), "A micromechanical approach to elastic and viscoelastic properties of fiber reinforced concrete", *Cement Concrete Res.*, **40**(3), 460-472. https://doi.org/10.1016/j.cemconres.2009.10.018.

Escarpini Filho, R.D.S. and Marques, S.P.C. (2016), "A model for homogenization of linear viscoelastic periodic composite materials with imperfect interface", *Lat. Am. J. Solid. Struct.*, **13**(14), 2706-2735. https://doi.org/10.1590/1679-78252749.

Fassi-Fehri, O. (1985), "Le problème de la paire d'inclusions plastiques et hétérogènes dans une matrice anisotrope: application à l'étude du comportement des matériaux composites et de la plasticité", Université Paul Verlaine-Metz.

Fisher, F.T. and Brinson, L.C. (2001), "Viscoelastic interphases in polymer-matrix composites: theoretical models and finite-element analysis", *Compos. Sci. Technol.*, **61**(5), 731-748. https://doi.org/10.1016/S0266-3538(01)00002-1.

Gillani, A. (2018), "Development of material model subroutimes for linear and non linear response of elastomers", University of Western Ontario, Ontario.

Hashin, Z. (1965), "Viscoelastic behavior of heterogeneous media", *J. Appl. Mech.*, **32**(3), 630-636. https://doi.org/10.1115/1.3627270.

Hashin, Z. (1970), "Complex moduli of viscoelastic composites-I. General theory and application to particulate composites", *Int. J. Solid. Struct.*, **6**(5), 539-552. https://doi.org/10.1016/0020-7683(70)90029-6.

Hu, A., Li, X., Ajdari, A., Jiang, B., Burkhart, C., Chen, W. and Brinson, L.C. (2018), "Computational analysis of particle reinforced viscoelastic polymer nanocomposites-statistical study of representative volume element", *J. Mech. Phys. Solid.*, **114**, 55-74. https://doi.org/10.1016/j.jmps.2018.02.013.

Jung, J., Park, C., Ryu, M.S. and Yun, G.J. (2021), "A molecular structure-informed viscoelastic constitutive model for natural rubber materials", *Funct. Compos. Struct.*, **3**(4), 045002. https://doi.org/10.1088/2631-6331/ac34fc.

Khan, M.M.K., Liang, R. Gupta, R. and Agarwal, S. (2005), "Rheological and mechanical properties of ABS/PC blends", *Korea-Australia Rheology J.*, **17**(1), 1-7.

Kim, Y., Jung, J., Lee, S., Doghri, I. and Ryu, S. (2022), "Adaptive affine homogenization method for Visco-hyperelastic composites with imperfect interface", *Appl. Math. Model.*, **107**, 72-84. https://doi.org/10.1016/j.apm.2022.02.007.

Kitey, R. and Tippur, H. (2005), "Role of particle size and filler–matrix adhesion on dynamic fracture of glass-filled epoxy. I. Macromeasurements", *Acta Materialia*, **53**(4), 1153-1165. https://doi.org/10.1016/j.actamat.2004.11.012.

Kolahchi, R. and Cheraghbak, A. (2017), "Agglomeration effects on the dynamic buckling of viscoelastic microplates reinforced with SWCNTs using Bolotin method", *Nonlin. Dyn.*, **90**(1), 479-492. https://doi.org/10.1007/s11071-017-3676-x.

Lahellec, N. and Suquet, P. (2007), "Effective behavior of linear viscoelastic composites: A time-integration approach", *Int. J. Solid. Struct.*, **44**(2), 507-529. https://doi.org/10.1016/j.ijsolstr.2006.04.038.

Laws, N. and McLaughlin, R. (1978), "Self-consistent estimates for the viscoelastic creep compliances of composite materials", *Proc. Roy. Soc. London Ser. A*, **359**(1697), 251-273. https://doi.org/10.1098/rspa.1978.0041.

Le, Q., Meftah, F., He, Q.C.and Le Pape, Y. (2007), "Creep and relaxation functions of a heterogeneous viscoelastic porous medium using the Mori-Tanaka homogenization scheme and a discrete microscopic

retardation spectrum", *Mech. Time-Depend. Mater.*, **11**(3-4), 309-331. https://doi.org/10.1007/S11043-008-9051-Z.
Li, J. and Weng, G.J. (1994), "Strain-rate sensitivity, relaxation behavior, and complex moduli of a class of isotropic viscoelastic composites", *J. Eng. Mater. Technol.*, **116**(4), 495-504. https://doi.org/10.1115/1.2904319.
Li, K., Gao, X.L. and Roy, A.K. (2006), "Micromechanical modeling of viscoelastic properties of carbon nanotube-reinforced polymer composites", *Mech. Adv. Mater. Struct.*, **13**(4), 317-328. https://doi.org/10.1080/15376490600583931.
Liu, Z. (2017), "Reduced-order homogenization of heterogeneous material systems: from viscoelasticity to nonlinear elasto-plastic softening material", Northwestern University.
Molinari, A., Ahzi, S. and Kouddane, R. (1997), "On the self-consistent modeling of elastic-plastic behavior of polycrystals", *Mech. Mater.*, **26**(1), 43-62. https://doi.org/10.1016/S0167-6636(97)00017-3.
Müller, M. (2017), "Mechanical properties of resin reinforced with glass beads", *Agron. Res.*, **15**(S1), 1107-1118. https://doi.org/10.1177/096739111802600105.
Paipetis, S.A. and Grootenhuis, P. (1979), "The dynamic properties of particle reinforced viscoelastic composites", *Fib. Sci. Technol.*, **12**(5), 377-393. https://doi.org/10.1016/0015-0568(79)90004-6.
Pan, Z., Huang, R. and Liu, Z. (2019), "Prediction of the thermomechanical behavior of particle reinforced shape memory polymers", *Polym. Compos.*, **40**(1), 353-363. https://doi.org/10.1002/pc.24658.
Patnaik, S.S., Swain, A. and Roy, T. (2020), "Creep compliance and micromechanics of multi-walled carbon nanotubes based hybrid composites", *Compos. Mater. Eng.*, **2**(2), 141. https://doi.org/10.12989/cme.2020.2.2.141.
Qu, J. (1993), "The effect of slightly weakened interfaces on the overall elastic properties of composite materials", *Mech. Mater.*, **14**(4), 269-281. https://doi.org/10.1016/0167-6636(93)90082-3.
Ricaud, J.M. and Masson, R. (2009), "Effective properties of linear viscoelastic heterogeneous media: Internal variables formulation and extension to ageing behaviours", *Int. J. Solid. Struct.*, **46**(7), 1599-1606. https://doi.org/10.1016/j.ijsolstr.2008.12.007.
Rodríguez-Ramos, R., Otero, J. A., Cruz-González, O. L., Guinovart-Díaz, R., Bravo-Castillero, J., Sabina, F. J., ... & Sevostianov, I. (2020), "Computation of the relaxation effective moduli for fibrous viscoelastic composites using the asymptotic homogenization method", *Int. J. Solid. Struct.*, **190**, 281-290. https://doi.org/10.1016/j.ijsolstr.2019.11.014.
Sevostianov, I., Levin, V. and Radi, E. (2016), "Effective viscoelastic properties of short-fiber reinforced composites", *Int. J. Eng. Sci.*, **100**, 61-73. https://doi.org/10.1016/j.ijengsci.2015.10.008.
Shokrieh, M.M., Ghajar, R. and Shajari, A.R. (2016), "The effect of time-dependent slightly weakened interface on the viscoelastic properties of CNT/polymer nanocomposites", *Compos. Struct.*, **146**, 122-131. https://doi.org/10.1016/j.compstruct.2016.03.022.
Tchalla, A., Azoti, W.L., Koutsawa, Y., Makradi, A., Belouettar, S. and Zahrouni, H. (2015), "Incremental mean-fields micromechanics scheme for non-linear response of ductile damaged composite materials", *Compos. Part B: Eng.*, **69**, 169-180. https://doi.org/10.1016/j.compositesb.2014.08.055.
Vieville, P., Bonnet, A. and Lipiński, P. (2006), "Modelling effective properties of composite materials using the inclusion concept. General considerations", *Arch. Mech.*, **58**(3), 207-239.
Vieville, P., Bonnet, A.S. and Lipiński, P. (2006), "Modelling effective properties of composite materials using the inclusion concept. General considerations", *Arch. Mech.*, **58**(3), 207-239.
Zhao, W., Liu, L., Leng, J. and Liu, Y. (2019), "Thermo-mechanical behavior prediction of particulate reinforced shape memory polymer composite", *Compos. Part B: Eng.*, **179**, 107455. https://doi.org/10.1016/j.compositesb.2019.107455.
Zhu, X.Y., Wang, X. and Yu, Y. (2014), "Micromechanical creep models for asphalt-based multi-phase particle-reinforced composites with viscoelastic imperfect interface", *Int. J. Eng. Sci.*, **76**, 34-46. https://doi.org/10.1016/j.ijengsci.2013.11.011.